Corrosion Science 200 (2022) 110252

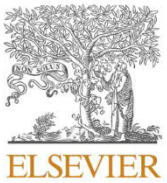

Contents lists available at ScienceDirect

Corrosion Science

journal homepage: www.elsevier.com/locate/corsci

Organic composite coatings containing mesoporous silica particles: Degradation of the SiO_2 leading to self-healing of the delaminated interface

Yue Yin, Huan Zhao, Manoj Prabhakar, Michael Rohwerder *

Max-Planck-Institut für Eisenforschung GmbH, 40237 Düsseldorf, Germany

ARTICLE INFO

Keywords:
Corrosion protection
Self-healing
Mesoporous silica
Cathodic delamination
Hybrid coatings

ABSTRACT

Mesoporous SiO_2 is of interest as nano-container for storing active agents for corrosion inhibition or self-healing. However, the potential of mesoporous SiO_2 itself for providing active corrosion protection so far was widely ignored. Here, SiO_2 containing PVB coatings applied on zinc is shown to inhibit corrosion-driven organic coating disbondment and even to self-heal the already delaminated interface. The protection mechanism is that mesoporous SiO_2 will degrade in the high alkaline pH at the delaminated area and forms a silicate layer that blocks underfilm corrosion and even re-establishes a protective and delamination resistant interface.

1. Introduction

Organic coatings are an efficient method used for the protection of metallic substrates, which are of great importance in industry applications [1–5]. First of all, a coating acts as a physical barrier inhibiting the contact between the corrosive medium, especially its aggressive ions, and the metallic substrate. However, organic coatings without additives usually cannot offer reliable long-term adequate protection of the metallic substrate from corrosion. Hence, adding organic or inorganic filler into the organic coating matrix to improve its passive performance (increasing its barrier function) and also to add active corrosion protection is attracting intense research [6–9].

Of crucial importance is added active corrosion protection [7,10]. To further improve the performance of the organic coating, corrosion inhibiting species are added to its matrix. The idea is that once the coating gets less protective and corrosion starts, corrosion inhibitors can slowly leach out, if possible on demand, to passivate the damaged areas. The inhibitive mechanism is that corrosion inhibitors will react with the metallic substrate (or ions released from it by corrosion) to form corrosion protection layers covering the substrate surface. However, for standard pigments designed for leaching of corrosion inhibitor, the inhibitor will be released when exposed to humid environment, even without corrosion occurring. That means this leaching process is uncontrolled, not on demand, and the steady loss of inhibitor and will shorten the lifetime of the corrosion protection.

Of course, also improving the passive barrier effect is of importance. The incorporation of inorganic nanoparticles into the coating matrix can significantly improve its performance and thus prolong the service life of the organic coating [11–18]. The mechanism of improving the passive corrosion resistance is that the inorganic nanoparticles can improve the degree of crosslinking within the coating, occupy pores and cavities existing in the coating matrix, and by generally extending the pathway for the diffusion of aggressive ions. All this extends the time for diffusion of corrosive species to the interface between coating and metallic substrate. Silica nanoparticles are especially attractive, because they are quite simple to synthesize and their good compatibility with most coating materials. A lot of work was done to study the effect of silica size, surface hydrophobic as well as hydrophobic silica on organic coating corrosion properties. Xu [11] et al. incorporated hydrophobic nano-silica and hydrophilic nano-silica into epoxy coating to evaluate the corrosion resistance. Compared with the coating containing hydrophilic nano-silica, the coating with incorporated hydrophobic nano-silica showed a better anticorrosive performance. The addition of hydrophobic nano-silica to the coating was proposed to effectively prolong the diffusion path of aggressive ions and water by filling the pores, thus improving the quality of the coating. Song [12] et al. studied the effects of the size of nano-silica as well as of silica content on the corrosion resistance of a fluoropolymer-silica coating. They emphasized that the size of silica plays an important role in dispersive capacity and improving the corrosion resistance of the coated steel. The silica with a mean diameter of 150 nm showed good dispersive capacity and corrosion protection. El-Ghazawy [13] et al. prepared silica epoxy composite coatings with nano silica and micro silica using ultrasonic technique. A uniform dispersion epoxy-silica coating was obtained with a maximum

* Corresponding author.
E-mail address: rohwerder@mpie.de (M. Rohwerder).

https://doi.org/10.1016/j.corsci.2022.110252
Received 29 November 2021; Received in revised form 15 March 2022; Accepted 16 March 2022
Available online 19 March 2022

added amount of less than 3%. The results showed that the micro-silica containing coating has higher hydrophobicity than the coating with added nano-silica. However, addition of nano-silica in epoxy can nerveless improve the corrosion resistance compared to micro-silica containing coating. This is attributed to good dispersion of the silica in the epoxy coating matrix, which results in a compact structure, and also seems to improve the adhesion of the epoxy coating to the metallic substrate. Xin [14] et al. added various amounts of silica nanoparticles into a silane functionalized polybenzoxazine coating to improve the coating's corrosion resistance. It was found that silica containing coatings showed a remarkable improvement of corrosion resistance, which they attributed to a synergistic effect of increased barrier properties and anodic inhibition induced by the formation of passive Fe-silicate compounds. Wang [15] et al. investigated the effect of the co-incorporation of Na-montmorillonite (MMT) and mesoporous silica MCM-41 into epoxy matrix on the corrosion properties. The results showed that coating containing the two types of filler showed significantly improved performance, supposedly by efficient filling of small pores, improving the barrier properties of the nanocomposite coatings, which is furthermore also additionally ascribed to an improved cross-linking. Ferreira [16] et al. reported that bis-[triethoxysilylpropyl] tetrasulfide (BTESPT) mixed with microparticles of silica pretreated on hot dip galvanized steel can significantly improve the corrosion protection in comparison to pretreatment with BTESPT only. The good performance was ascribed to a higher silane film thickness and/or decrease of the porosity of coating. Van Ooij [17] et al. showed that by adding silica to silane films on AA 2024-T3 a higher film thickness and lower porosity can be achieved, leading to significantly enhanced corrosion protection. They proposed that the silica reacts with cathodically generated OH^-, resulting in its degradation and the formation of SiO_3^{2-} which then reacts with Al^{3+} at the anode to form a corrosion inhibiting Al-silicate compound layer. Furthermore, in immersion experiments they observed that the corrosion potential shifted to the more cathodic direction, which they proposed to indicate that the silica containing coating can effectively inhibit the cathodic reaction. The work emphasizes that the corrosion performance is dependent on the amount of silica. Fernández-Álvarez [18] et al. studied the effect of incorporation of two different silica (hydrophilic, HL, and hydrophobic, HB) on the corrosion performance of an epoxy coating on carbon steel measured by SKP. The coating containing HB is more efficient to slow down water absorption into and permeation through the coating than the one containing HL. The HB containing coating was also observed to be more effective than HL in delaying the progress of cathodic delamination.

Although adding active pigments or inorganic inert nanoparticles can improve the corrosion resistance of organic coatings, both methods have their drawbacks. For standard active pigments the leaching from the coating is uncontrolled and inert inorganic nanoparticles just improve the strength and barrier properties of coating and cannot repair an inflicted defect. Hence, there is a widespread activity in designing and developing environmentally friendly coatings featuring a smart on demand release of corrosion inhibitor only when active corrosion occurs. Adding switchable nanocontainers or capsules containing corrosion inhibitor into the coating matrix are one idea for realizing such smart self-healing coatings [19,20,26]. Among the inorganic nanocontainers, mesoporous SiO_2 is widely studied due to properties such as high loading capacity, large surface area and controllable pore diameter. Aoki [21] et al. prepared dodecylamine loaded mesoporous silica SBA-15 particles and embedded them into an alkyd primer to evaluate active corrosion protection of carbon steel. The dodecylamine-loaded SBA-15 nanocontainer was not only claimed to block the defects, improving the physical barrier properties of the alkyd primer coating, but also the release of dodecylamine from the SBA-15 was observed to provide active corrosion protection. Due to the release of dodecylamine, a significant increase of the active anticorrosion properties was observed.

In order to further control the release of corrosion inhibitor, the nanocontainers are assembled with different gatekeeper encapsulation layers which can be triggered by different external or internal factors (pH change, mechanical damage, etc.) [22]. The encapsulation serves to prevent spontaneous corrosion inhibitor leakage from the nanocontainers, thus achieving more efficient and economical use of the inhibitor. These gatekeepers only open the nanocontainers when a defect site starts to actively corrode. Then release of corrosion inhibitors to the corrosion site will occur. Corrosion inhibitor transport to the defect as an important parameter was studied in our previous work [23]. Concerning suitable gatekeepers, there is quite a number of reports on possible strategies to prevent spontaneous release without external trigger. Zhang [24] et al. prepared a shape memory epoxy coating matrix containing TiN@mesoporous SiO_2 core-shell nanocontainers loaded with benzotriazole (BTA). The results revealed that this dual-action self--healing protective coating, under a near-infrared light trigger, the thermogenesis effect of TiN can promote the release of BTA from the mesoporous silica. Thus, not only the corrosion in the defect is inhibited, but the triggered shape memory effect also merges the damaged epoxy coating in the scratch. Shchukin [25] et al. designed layer-by-layer (LbL)-assembled polyelectrolyte multilayers as pH triggered gate over the nanocontainer outermost surface to prepare corrosion inhibitor 2-(benzothiazol-2-ylsulfanyl)-succinic acid containing mesoporous silica nano-reservoirs. The idea is that the corrosion inhibitor is sealed within the polyelectrolyte multilayers during the LbL-assembly step, but this encapsulation gets porous when the pH changes. Such prepared nano-reservoirs were mixed into silica-zirconia-based hybrid film as a coating matrix, applied on AA2024 aluminum alloy substrate and the release of corrosion inhibitor initiated by pH changes, which occur when the corrosion starts, was investigated. The sol-gel coating containing nanocontainers demonstrates enhanced long-term corrosion protection in comparison with the silica-zirconia-based hybrid coating without the nano-reservoirs, due to the release of the corrosion inhibitor triggered by the corrosion processes started in the cavities.

Many more interesting works were done on mesoporous particles for corrosion protection, providing promising results especially on smart self-healing [21,24,25]. However, for designing nano-containers for application in self-healing coatings, choosing the best nano-containers support is also one of most challenge works. For mesoporous SiO_2, the suitability for storage of inhibitor has been investigated extensively [21, 24,25], as well as possible smart encapsulation strategies and the performance.

However, the contribution of the degradation of the mesoporous SiO_2 itself during the corrosion process on the overall inhibition was neglected so far, especially concerning a possibly beneficial role at the polymer/metal interface where high concentrations of degradation products of the silica can be expected in the alkaline environment of the delaminating interface. The aim of this work is to provide insight into this by combined chemical analysis and in-situ SKP measurement to study the degradation of mesoporous SiO_2 added to organic coating -especially at the delaminating interface- and how this may affect the interaction the between the organic coating and the metallic substrate. As will be shown, the degrading silica can cause significant self-healing of the delaminating and the delaminated interface on zinc and hence may play an important role for improved self-healing of coatings applied onto galvanized steel. In earlier works we have already shown that coating delamination is both very efficient in spreading the trigger signal for release as well as providing fast transport [27,28]. Efficient self-healing of the delaminated interface is of crucial importance once the defect is inhibited and healed. Silica could play an important role here.

2. Materials and methods

2.1. Materials

Iron and zinc sheets (99.95%) were purchased from Goodfellow. The

specimens were cut to a size of 20 mm×10 mm and subsequently ground with SiC paper, cleaned with water and ethanol, and dried under a nitrogen stream. Potassium chloride (KCl, purity 99%), sodium hydroxide (NaOH, ≥98%), cetyltrimethylammonium bromide (CTAB), ethanol, potassium hydroxide (KOH, ACS reagent, ≥85%), methanol (anhydrous, 99.8%), ethanol, tetraethyl orthosilicate (TEOS, 98%) and poly(vinyl butyral-co-vinyl alcohol-co-vinyl acetate) (PVB) (MW≈50000–80000 g/mol) were supplied by Sigma-Aldrich. A dialysis bag (MWCO 14000) was purchased from Sigma-Aldrich. An aqueous solution of HCl (Baker, 37%) was used to adjust the pH value of the reaction system. Mesoporous silica SBA-15 (rod-like with <150 μm particle length with about 200 nm diameter, hexagonal pore morphology) with a surface area 450–550 m^2/g and pore size 8 nm and mesostructured silica MCM-41 type (hexagonal) with a pore size 2.1–2.7 nm and specific surface area ~1000 m^2/g (BET, Brunauer-Emmett-Teller) were purchased from Sigma-Aldrich.

2.2. Synthesis of mesoporous silica nanoparticles (MSNP)

MSNP were prepared by a modified procedure of Lin [29] et al. In a typical preparation, 0.5 g CTAB was dissolved into 240 ml ultrapure water in a three neck round bottom flask, followed by adding 1.75 ml NaOH (2 M) solution. The above solution was heated in an oil bath at 80 °C with continuous stirring at 600 rpm. 2.5 ml TEOS were added dropwise under stirring for 2 h. The final products were collected by centrifugation, washed thoroughly with ultrapure water and methanol, and dried in air. To remove the CTAB, the raw product was put in a mixture solution of 160 ml methanol and 9 ml HCl (37.4%) was refluxed for 24 h. The resulting materials was centrifuged and washed with ultrapure water and methanol to yield the as-synthesized MSNP.

2.3. Composite coating preparation

Three types of coatings were studied: the PVB coating with added SBA-15, MCM-41 or MSNP, respectively. Mesoporous silica was mixed with 5% PVB in ethanol to achieve the targeted amount of silica in the coating, i.e. 0.5%, 1%, 2% and 4%. The thus obtained silica containing solutions were spin-coated 4 times at 2000 rmp for 20 s on Zn or Fe substrate and dried at 80 °C for 10 min. After drying the sample, the same procedure was used to apply 10% PVB as a topcoat for 3 times dried at 80 °C for 10 min

2.4. Characterization of the coating

Scanning electron microscopy (SEM, LEO 1550VP, Carl Zeiss) was used to characterize the morphology of mesoporous silica. Fourier transform infrared (FTIR) spectra were recorded with a Bruker Vertex 70 v Fourier transform IR spectrometer in the region 400–4000 cm^{-1}. Powder samples were prepared in the form of KBr pellets. An X-Ray Photoelectron Spectroscopy (XPS) (ESCA Quantum 2000 Microprobe) from PHI was used for surface analysis of the delaminated interface after removal of the PVB coating. For analyzing the Si and Zn concentration, high-resolution core level XPS spectra of Si and Zn were used. The XPS data were all processed and analyzed with CASA XPS software.

2.5. Degradation of mesoporous silica measurements

0.01 g mesoporous silica dispersions in 5 ml 1 M KCl solution were enclosed in a dialysis bag. The dialysis bag was immersion in 95 ml aqueous 1 M KCl solution. The pH of the KCl solution was adjusted with aqueous KOH solution to a pH value of 10. At specific interval times 1 ml of electrolyte was taken and the same volume of stock solution was added again into the above container. The concentration of Si was determined using an Inductively Coupled Plasma-Optical Emission Spectrometer (ICP-OES, Iris Intrepid Duo HR) from Thermo Fisher Scientific.

2.6. SKP Measurements

To study cathodic delamination, its progress was monitored in situ with by Scanning Kelvin Probe (SKP) technique [30]. For this a system from KM Soft Control was used. Prior to the corrosion testing, an artificial defect (2.5 mm ± 0.2 mm long, 30 μm ± 5 μm wide, and 42 μm ± 6 μm deep) was prepared into the coating with a razor blade. The defect was covered with 7.5 μl 1 M KCl and the sample was subsequently introduced into the SKP chamber with a relative humidity of 93%. The SKP tip was calibrated vs. $Cu/CuSO_4$ (saturated) and all potentials are referred to SHE. The experimental setup for measuring the cathodic delamination of the mesoporous silica containing coating via SKP is schematically shown in Fig. 1.

3. Results and discussion

3.1. Characterization of mesoporous silica

SEM images of SBA-15, MCM-41 and MSNP are shown in Fig. 2. The SEM images revealed a rod-like domains structure of SBA-15. The diameter size of the rod-like SBA-15 is ~0.2 μm and a relatively length range several to hundreds micrometer. The structures of SBA-15 is similar as reported in previous papers [31]. MCM-41 exhibits irregular spherical particles with diameters around 500 nm, but particles as big as 1 μm are detected as well. The MSNP particles show a homogeneous spherical morphology in both size and shape, with monodisperse spherical-shaped nanoparticles and an average diameter of particles below 200 nm.

Fig. 3 shows the FTIR spectra for SBA-15, MSNP and MCM-41 powder. The infrared spectra show that are typical of mesoporous silica. The peak at around 3430 cm^{-1} is attributed to the stretching vibration of adsorbed water molecules on the surface of the mesoporous silica, where the lower hydroxyl group intensity confirms the hydrophobicity of the SBA-15 and MCM-41 particles. Correspondingly, the peak at around 1630 cm^{-1} is due to the bending vibration of water on the mesoporous silica, where also the intensity of the MNSP peak is stronger than the SBA-15 and the MCM-41 and it demonstrates the former one is hydrophilic mesoporous silica. The signal at around 1080 cm^{-1} is attributed to asymmetric vibrations of Si—O—Si. The signal at 810 cm^{-1} is belong to stretching symmetric vibrations of Si—O. The band at 460 cm^{-1} is attributed to the bending vibration or rocking mode of Si—O—Si [32,33]. However, MSNP has a peak at 963 cm^{-1} which most like is associated with Si—OH and is not observed for the other two mesoporous silica. The strong peaks at the 3430 cm^{-1} and 963 cm^{-1} indicate that the MSNP is a hydrophilic particle.

Fig. 4 shows FTIR spectra of PVB, SBA-15 and the PVB-SBA-15 composite coating. Fig. 4(a) shows the spectra of PVB powder (in KBr pellet) and of PVB coating applied onto zinc substrate. The absorption peak at 3440 cm^{-1} signifies the stretching vibration of hydroxyl group of PVB powder or water molecular. However, a much broader peak from

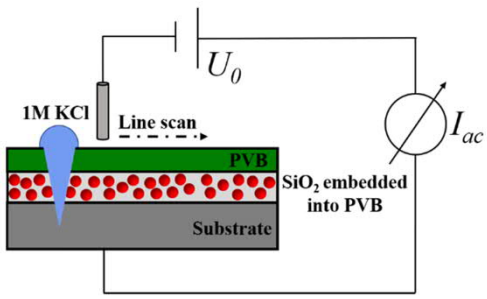

Fig. 1. Scheme of the model-coating system and the set-up used to study the cathodic delamination (not to scale). Here the coating is shown to be PVB with added silica, covered with a PVB top-coating.

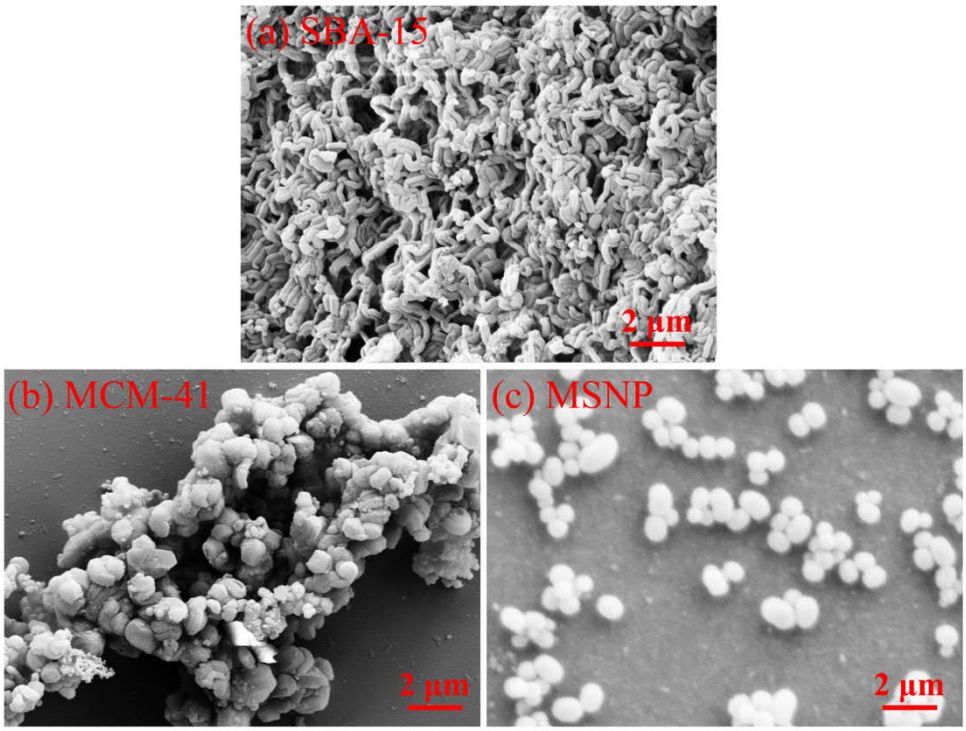

Fig. 2. SEM images of mesoporous silica particle. (a) SBA-15, (b) MCM-41, (c) MSNP.

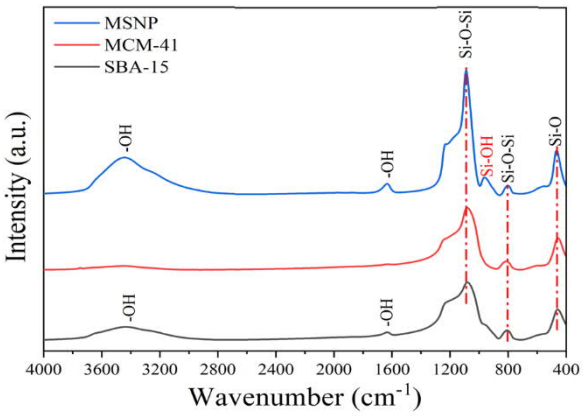

Fig. 3. FTIR spectra of different mesoporous silica power.

the 4000–2000 cm^{-1} represents the hydroxyl group and C−H stretching for the PVB coating, which is prepared from PVB powder mixed into ethanol and then coated on zinc substrate. The bands in the range 2850 cm^{-1} to 3000 cm^{-1} represent the aliphatic C−H stretching. The peak at 1731 cm^{-1} is attributed to the stretching vibration of C═O. The peaks 1432 cm^{-1} and 1380 cm^{-1} correspond to asymmetry stretching CH_2 and CH_3 group bending, respectively. The peaks at 1344 cm^{-1} and 808 cm^{-1} are due to C—H symmetry stretching. The bands at 1100 cm^{-1} and 1056 cm^{-1} are assigned to C—O—C—O—C stretching. The band at 1240 cm^{-1} and 1010 cm^{-1} are ascribed to C—O—C stretching. These peaks are the typical bands of PVB powder [34–36]. However, the peaks of the C—O—C—O—C and C—O—C stretching shift to the 1140 cm^{-1} and 1000 cm^{-1} for the PVB coating, respectively.

In Fig. 4(b) no indications for chemical interaction between the silica and the PVB can be seen for the SBA-15 mixed into the PVB coating. Only very small shifts are observed for some peaks and no new peaks appear. Comparison of major characteristic spectral peaks of the PVB-SBA-15 composite coating and SBA-15 reveals that all characteristic peaks of SBA-15 can be found also in the PVB-SBA-15 composite coating. The FTIR spectra of SBA-15 mixed with PVB are dominated by the Si—O—Si absorptions appearing at 1080 and 460 cm^{-1}, while a weak Si—O—Si peak is observed at 810 cm^{-1}. One more point is that the intensity of absorption peak of Si—O—Si at 460 cm^{-1} gradually increases with the increasing content of SBA-15 in the PVB from 0.5% to 4%. The characteristic peaks around the 1160 cm^{-1} and 1056 cm^{-1} for the C—O—C—O—C and C—O—C stretching of PVB coating can also be seen for PVB-SBA-15 composite coating, although the positions are slightly shifted. All that together indicates that the segmented structure of PVB coating is not affected by the presence of SBA-15, i.e. that SBA-15 can be successfully introduced into the PVB matrix without much change of the chemical structure of the PVB matrix [37,38].

3.2. Corrosion-driven cathodic delamination

3.2.1. Delamination behavior of PVB coating applied on zinc and iron

Prior to evaluation of the performance of the pigmented PVB coatings, the cathodic delamination kinetics of an unpigmented PVB coating were measured as a benchmark. Fig. 5 displays the potential profiles of PVB coatings applied on zinc and iron sheet as obtained by SKP. The corrosion driven cathodic delamination of PVB coated zinc or iron has been published on numerous occasions previously [27,28,39–44] and will be discussed here only briefly.

Here, a sigmoidal shape also called delamination front represents the boundary of the intact coating and the delaminated area, which is characteristic for the cathodic driven delamination of organic coatings on zinc and iron. Fig. 5(a) shows that in the undelaminated region of the sample the potential range ca. − 0.6 to − 0.4 V_{SHE}, which indicates the zinc is in its passive range (see e.g. [45]). Conversely, after the coating delaminated, the potential falls to the one of freely corroding zinc (ca. −0.8 V_{SHE}). For the iron sample coated with unpigmented PVB, the potentials in the intact regions range ca. between − 0.1–0.1 V_{SHE}, whereas the potential of the delaminated area is polarized by the defect to ca − 0.4 V_{SHE}, both these values being consistent with previous reported ones [40,43]. The delamination kinetic of PVB coated iron and zinc show the well-known sqrt(t) dependence reported before for PVB on

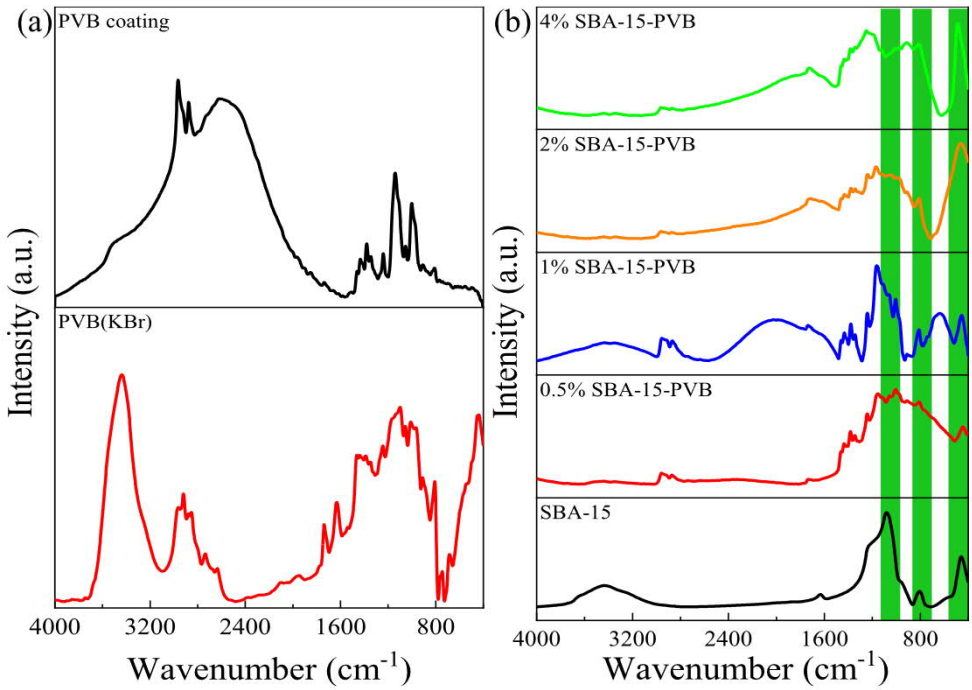

Fig. 4. FTIR spectra of (a) PVB powder in KBr and PVB coating, (b) KBr of SBA-15 and SBA-15 mixed into PVB coated coatings on Zn substrate. Green shading highlights the position of characteristic peaks of the SBA-15.

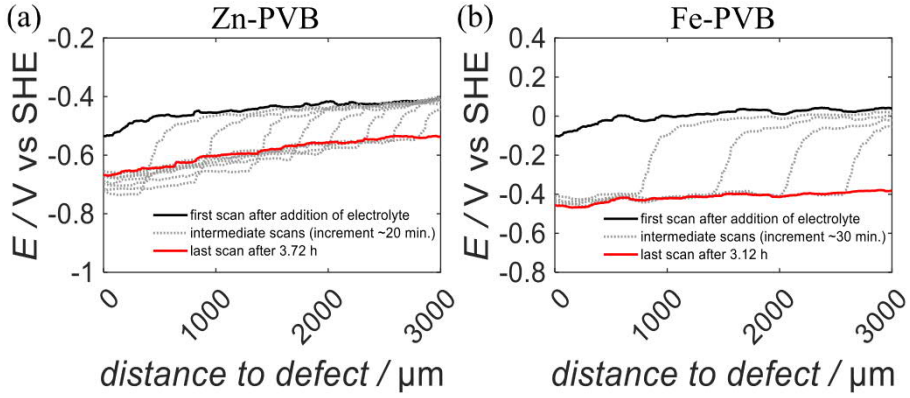

Fig. 5. Delamination profiles of PVB on a grounded metallic sheet. The artificial defect was filled with aqueous 1 M KCl solution. (a) Zinc substrate, (b) Iron substrate.

iron and zinc [27,39–42].

3.2.2. *Delamination behavior of PVB coating containing mesoporous SiO_2 on Zn*

Scanning Kelvin probe (SKP) studies have been used here to reveal the influence of mesoporous SiO_2 on the cathodic delamination kinetics at the polymer/metal interface. First cathodic delamination of PVB coatings containing the different types of mesoporous SiO_2 was investigated for such composite coatings on zinc. Typical delamination profiles are shown in Fig. 6 and Fig. 7. The effect of mesoporous SiO_2 on the rate of cathodic delamination of the PVB coating was investigated by systematically changing the amount of mesoporous SiO_2 added into the coating from 0.5% to 2%. In general, as shown in Fig. 5 the intact coating potential of uninhibited PVB coated Zn is almost − 400 mV_{SHE}, while the potential of the corroding defect is about − 800 mV_{SHE}. For the mesoporous SiO_2 containing PVB coating, the potential of intact coating is in the range of − 200 mV_{SHE} to − 400 mV_{SHE}, which can be directly correlated with values measured for Zn in a passive state. Hence, there is no significant variation of the potential of the intact coating containing mesoporous SiO_2 additions when compared with the unpigmented PVB sample, suggesting that the presence of mesoporous SiO_2 in the PVB has only minimal effect on the steady-state delamination-cell potentials, but it is obvious that there is a tendency towards slightly higher potentials. Upon onset of cathodic delamination, the delaminated area is polarized towards the potential of the defect, but now an effect of the kind of added silica and of different amounts becomes visible.

The addition of 0.5% MSNP to the PVB shows the typical cathodic delamination behaviour, where the delaminated area has a potential close to the potential of the defect. The coatings containing 0.5% mesoporous SiO_2 of SBA-15 or MCM-41 show initially also a typical delamination behaviour, but only for the first few hours. Then the potential of the delaminated area shifts into the more positive direction. This means that the delaminated area was not only passivated but also the interface was healed out, i.e. the galvanic coupling to the actively corroding defect was cut off by re-establishment of a high resistance against ion mobility. After a certain time, the potential of the delaminated area reaches the potential of the intact area again. That means that the delaminated area was fully turned into a new intact interface again,

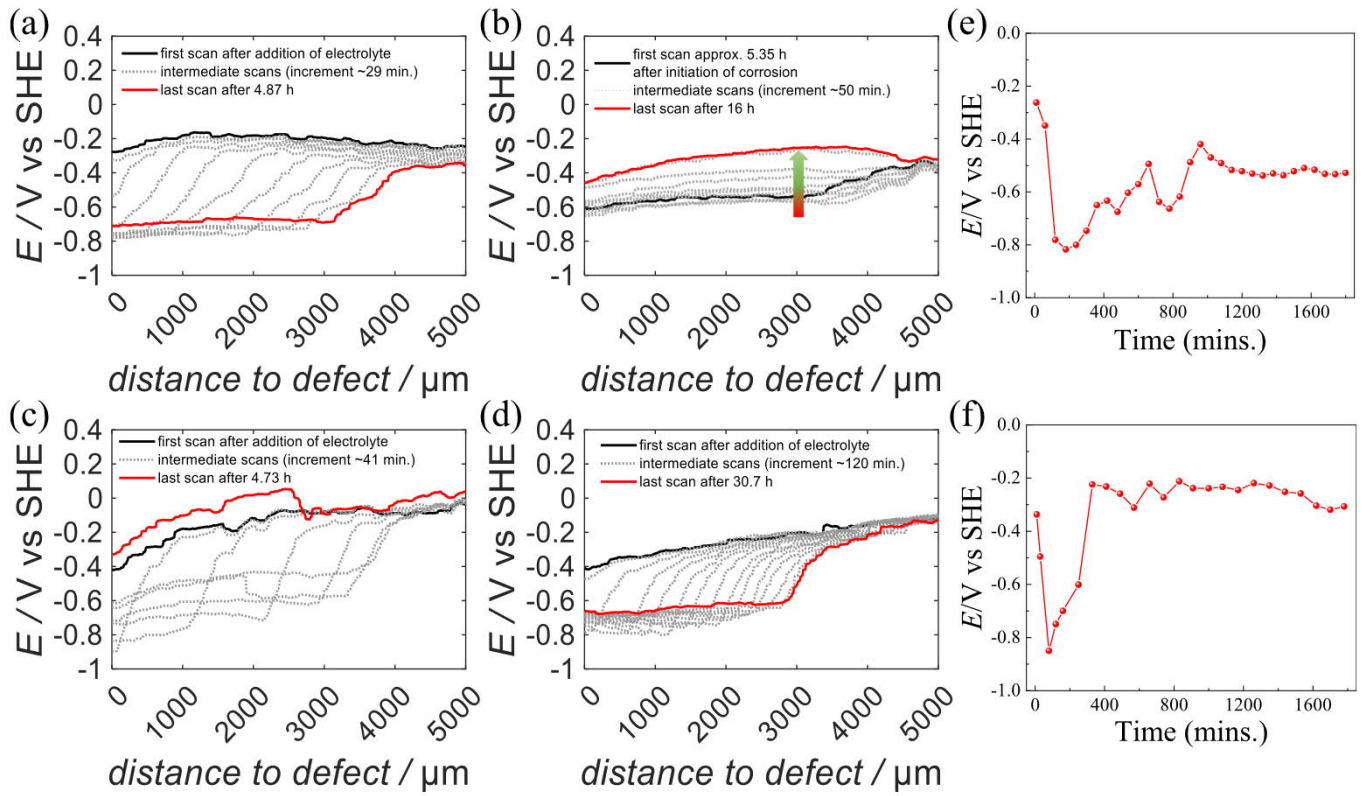

Fig. 6. Potential profiles measured during cathodic delamination of PVB coatings applied on zinc, containing 0.5% mesoporous silica; the artificial defect was filled with aqueous 1 M KCl solution. (a, b) MCM-41, (c) SBA-15, (d) MSNP. (e, f) The potential evolution at the delaminating and delaminated interface at x = 500 µm for the PVB-MCM-41(from (a) and (b)) and PVB-SBA-15 (from (c)).

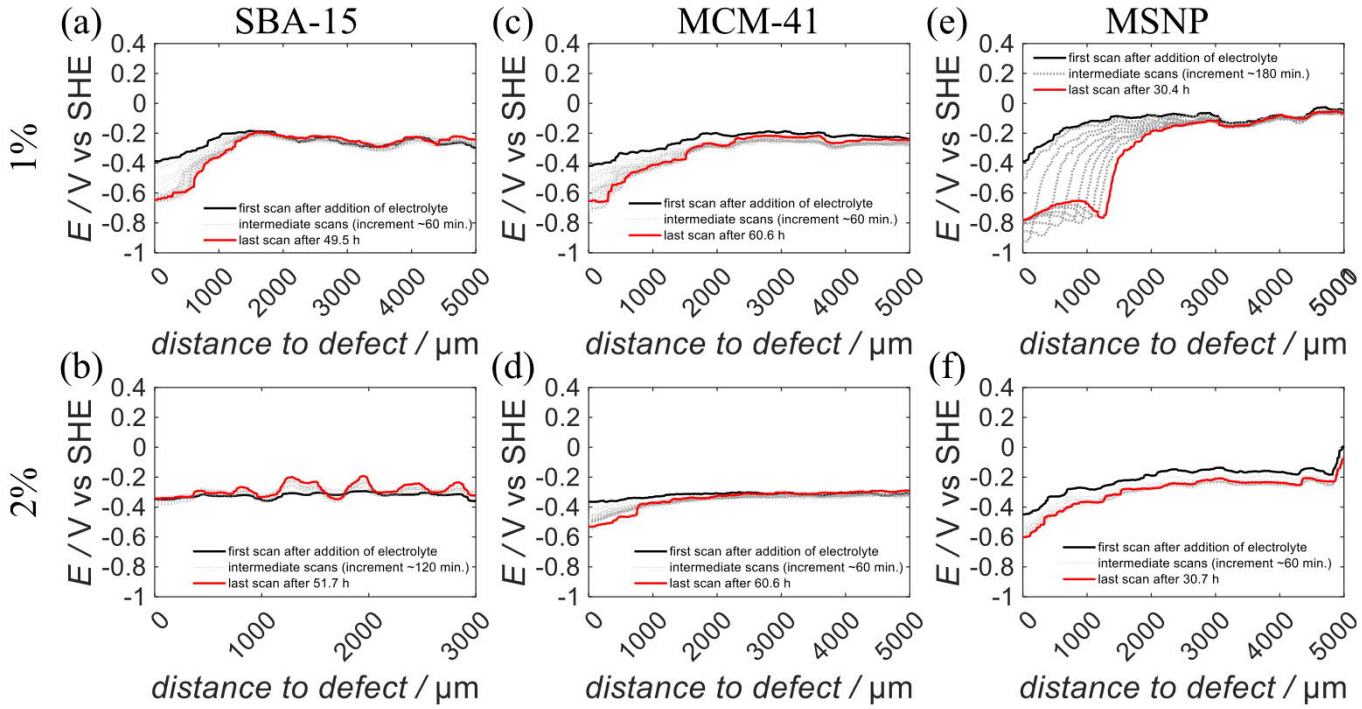

Fig. 7. Potential profiles measured during cathodic delamination of PVB coatings applied on zinc, containing different amounts of mesoporous silica; the artificial defect was filled with aqueous 1 M KCl solution. (a, b) SBA-15, (c, d) MCM-41, (e, f) MSNP.

i.e. real self-healing occurred. This self-healing is obviously linked to the degrading silica, as without it is not observed, i.e. just zinc hydroxide precipitation at the interface, as it might occur at later stage of delamination, cannot be the reason [46,47].

In order to better visualize the self-healing at the delaminated interface for 0.5% PVB-MCM-41 and PVB-SBA-15 applied on zinc, the

potential evolution at x = 500 μm is plotted as a function of time in Fig. 6(e, f). First the potential at the interface decreases due to the progress of delamination. Then an increase indicates onset of self-healing at the interface. The PVB coating containing SBA-15 shows a faster passivation and self-healing of the delaminated surface than the one containing MCM-41.

Interestingly, for higher additions of silica a further significant decrease in cathodic delamination rate is observed, but no self-healing of the delaminated interface. In fact, additions of 1% of SBA-15 or MCM-41 to the PVB resulted in more or less full inhibition of cathodic delamination, as can be seen in Fig. 7(a and c). Only initially some partial cathodic delamination seems to be initiated, but is quickly stopped. This could be explained by the need for an alkaline pH driven degradation of silica in order to form an inhibiting interface, i.e. delamination had to occur at least initially in order to cause the formation of a highly protective interface, which should accordingly be restricted to the delaminated interface. With increasing the additions to 2% SBA-15 or MCM-41 in the PVB coatings, no delamination front was observed during a comparable time of exposure. Also, here at least some initial delamination is expected to occur in order to allow the inhibitive effect of the silica to be built up, but that is assumed to be restricted to a region very close to the defect, which is not accessible for scanning with SKP (due to the proximity to the defect) and hence not visible here. That means that for the coatings with higher silica additions the inhibitions set in much faster. Such instantaneous self-healing was also observed in an earlier work where an instantaneous formation of a new polymer at the interface lead to a similar inhibition of cathodic delamination [28]. While for 0.5% the process took some time, which resulted in considerable initial delamination (similar progress as for just PVB, see Fig. 8), before effective inhibition at the interface occurred, at 1% this was already much faster and at 2% so fast that no delamination was observable at all.

Compared with the coatings containing 0.5% MCM-41 or SBA-15, the delamination rate is significantly decreased for the coating containing the same amount of MSNP. This can clearly see from the Fig. 8, where shows the delamination distance as a function of the time. Even, with 1% MSNP addition to the PVB coating, the delamination rate just decreases more, but still no self-healing can be observed. Further increase to 2% MSNP addition results in no visible delamination in the monitoring range. This latter result is similar as the ones obtained for 2% SBA-15 or MCM-41 containing PVB coatings. Additions of 2% mesoporous silica to the PVB coating result in an efficient inhibition of cathodic delamination regardless of the kind of silica particles used.

Hence, although the cathodic delamination rate (see e.g. Fig. 8) is significantly decreased with increasing silica (MSNP) addition to the PVB, no increase in potential of the delaminated interface can be observed, different from the case for 0.5% additions of SBA-15 and MCM-41 into PVB. This is proposed to be due exactly to this fast and effective inhibition of cathodic delamination, as this will prevent massive silica degradation and zinc corrosion at the interface, which is proposed to prevent the formation of a self-healing corrosion product layer restoring a blocking interface. This means that a certain minimum cathodic activity is needed for a self-healing at the interface. It should be noted that a passivation of the defect is observed in no case, i.e. the silica addition has no effect across higher distances.

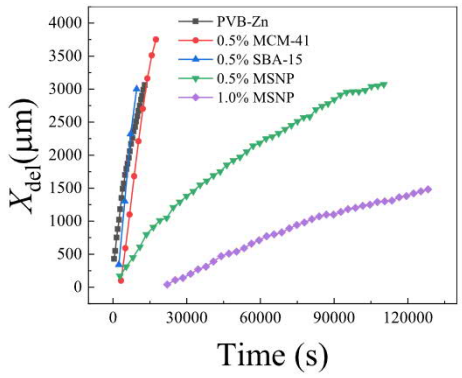

Fig. 8. The progress of the delamination front in air for plain PVB or PVB coating containing mesoporous silica of 0.5% and 1% on zinc plotted as function of time. The defect was covered by aqueous 1 M KCl solution. For 2% nearly total inhibition was observed. Hence, no progress is plotted here for above 1% silica content.

Another question now is why MSNP behaves so different from the other two particles. In view of both the FTIR analysis with the results obtained by SEM, the significant main differences of the MSNP to SBA-15 and MCM-41 are the particle size and its higher hydrophilicity, which maybe the main reason of the different passivation performance. It seems quite likely that the MNSP particles are highly accumulated at the PVB/metal(oxide) interface, which could possibly effectively decrease the delamination rate. This together with the small size of the MNSP might result also in less degraded silica, thus in less inhibition, even though initially faster inhibition of delamination progress. In this case, the more significant degradation of the mesoporous silica MCM-41 and SBA-15 are proposed to prompt the more significant passivation of the delaminated interface.

3.2.3. *Delamination behavior of mesoporous SiO_2 containing PVB on Fe*

In order to investigate whether the observed self-healing can be also observed on other substrates than zinc (or galvanized steel) and to further elucidate the protection mechanism also experiments on iron as substrate were performed. Typical cathodic delamination profiles obtained on iron for the three different types of mesoporous SiO_2 at different amounts added to PVB coating are shown in Fig. 9. The cathodic disbondment of unpigmented PVB on Fe is described and discussed in full detail elsewhere [39,40,43,48,49]. The delamination of PVB coatings with silica additions looks similar as without (see e.g. Fig. 5), but the delamination rate decreases with increasing silica content and the delamination progress changes from a sqrt(t) time dependence to a linear time dependence for silica additions above 0.5%. For PVB coating without any pigments applied on Fe, the potential of the intact area is in the range of 0–0.2 V_{SHE} and as can be seen from Fig. 9 the same is the case for PVB with additions of silica. When the coating starts to delaminate from the defect site into the intact coating, the potential under the delaminated area shifts towards the defect potential, which is about − 0.4 V_{SHE}. The results show that through incorporation of mesoporous silica into the PVB coating on Fe effectively decreases the delamination rate in comparison to the unpigmented PVB coating on Fe.

Fig. 10 shows the distance from the coating defect to the delamination front (X_{del}) plotted versus time. The rate of cathodic delamination was quantified by taking the position of the delamination front at the point of maximum potential gradient in the successive time-dependent E_{corr} profiles. In general, if the delamination rate varies linearly with the square root of time it is assumed that the delamination rate is controlled by the cation migration from the defect to the delamination front [50,51]. If the delamination rate is constant, i.e. delamination proceeds linearly with time, it is widely assumed that the oxygen reduction reaction is the rate-controlling process [52,53]. The here observed parabolic behavior for the delamination of PVB from zinc or iron is in agreement with previous reports [51,54]. For the mesoporous silica containing PVB coating on the iron substrate, with increasing mass fraction of silica the delamination rate is observed to decrease and also to change from parabolic (sqrt(t) kinetics) to linear (linear with respect to t) behavior become more and more visible. So, the for an amount of mesoporous silica in the PVB of more than 1%, the delamination process is linear, which might indicate that the oxygen reduction reaction is effectively suppressed and is now becoming the rate determining step. Similar performance was also reported by Williams et al. [39,41,42,44] for active pigment containing PVB on metallic substrate, where the cathodic delamination kinetics also changed from parabolic to linear kinetics for increased inhibition of delamination. Hence, the observed

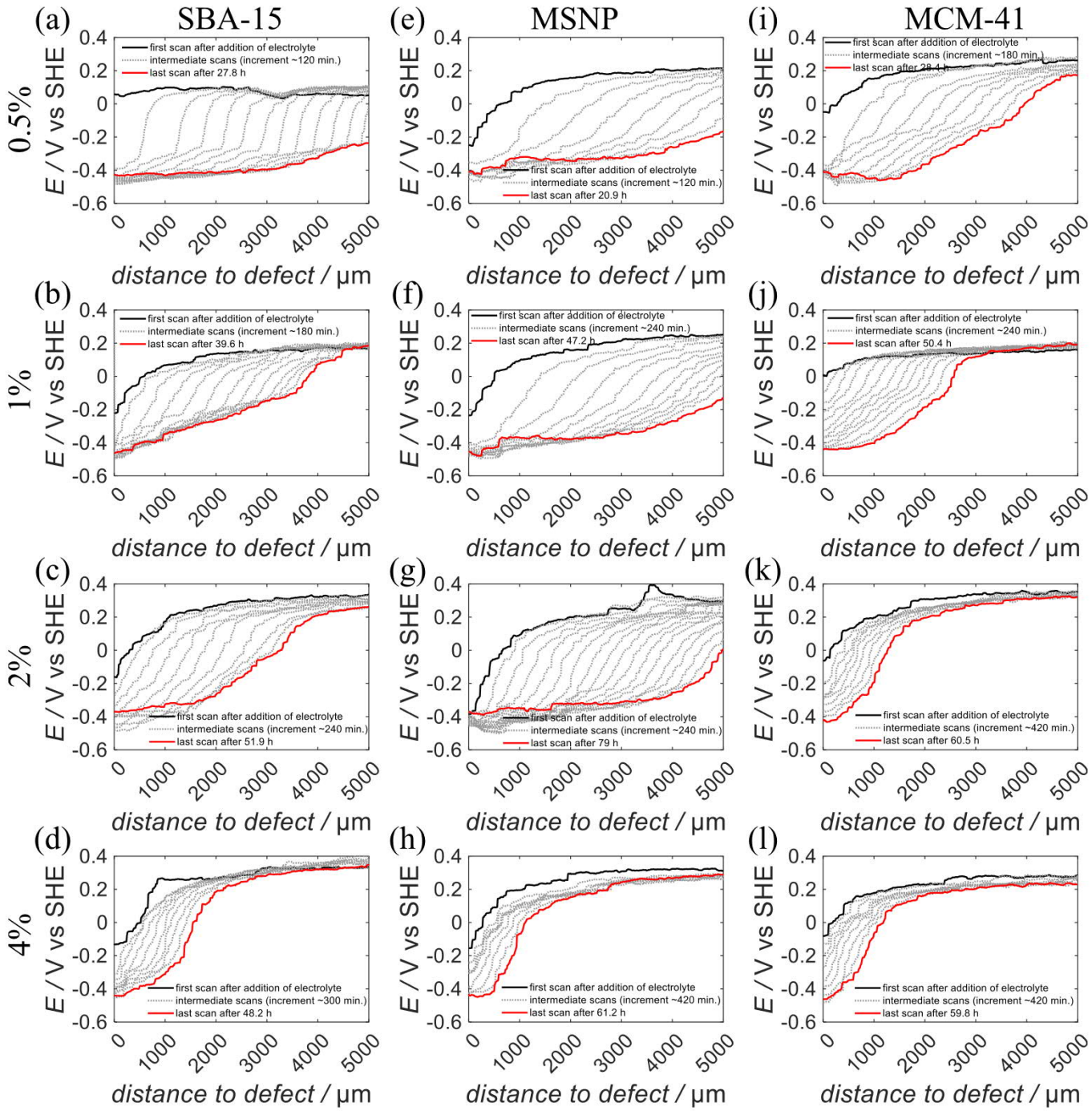

Fig. 9. Potential profiles measured by SKP for cathodic delamination of PVB coatings with additions of mesoporous silica applied onto Fe substrate. The defect was filled with aqueous1 M KCl solution. (a-d) SBA-15, (e-h) MSNP, (i-l) MCM-41.

change from sqt(t) like to linear behavior observed for increasing silica content in the PVB seems to be in good agreement with these assumptions. An active inhibiting role of the degradation products of the silica particles could be assumed that leads to the observed decrease in delamination rate as well to the change of kinetics. However, it shall be pointed out that recent reports indicate that these currently generally accepted views may not be correct and that new explanations for sqrt(t) and linear dependence have to be found [55].

Fig. 11 shows the average cathodic delamination rates of the PVB coatings containing different types and amounts of mesoporous silica coated on Fe substrate, determined from the delamination curves shown in Fig. 9. Please note that the kinetics of delamination change parabolic to linear behavior with increasing content of silica. This is why for a rough comparison the average rate over 30 h was taken here for comparison. For the 0.5% mesoporous silica containing PVB coating, the samples containing SBA-15 or MSNP show a much faster delamination than the PVB containing MCM-41. That demonstrates that size of and/or type of mesoporous silica have an influence on the delamination distance. Also, the amount of mesoporous silica incorporated into the PVB coating has an obvious effect on the delamination rate. Firstly, with increasing content of mesoporous silica from 0.5% to 4% in PVB coating, the delamination rate is even more significantly decreased. Secondly, for 4% silica content in the PVB, the delamination is quite similar for all three types of silica particles. For PVB containing 2% or 4% MCM-41, the

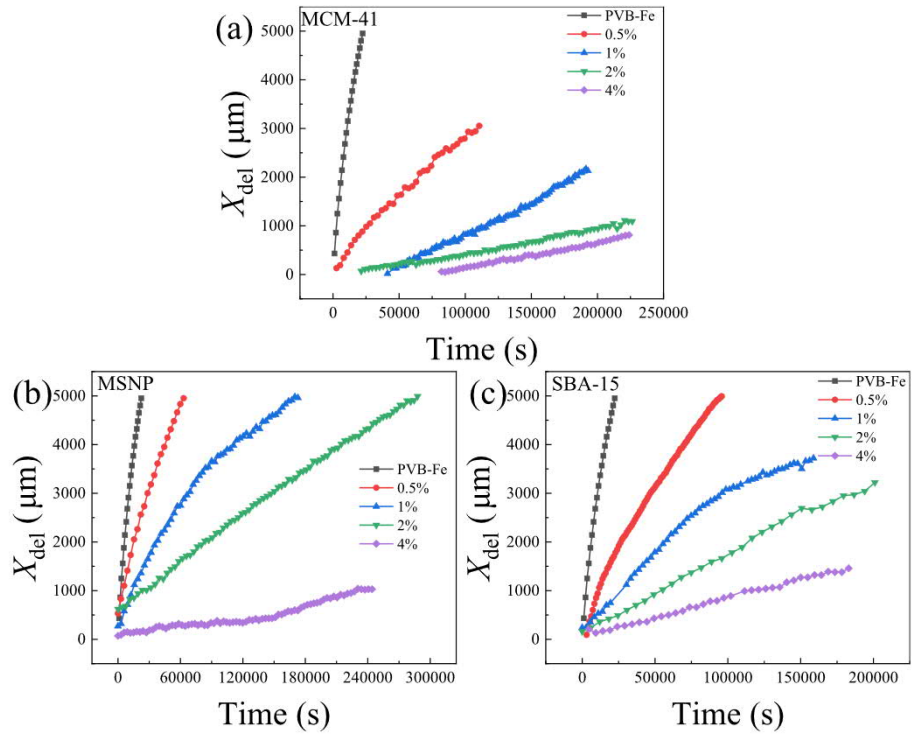

Fig. 10. Plots of delamination distance (X_{del}) as a function time for PVB films containing mesoporous silica mass fractions (%) of (a) SBA-15, (b) MSNP and (c) MCM-41 on iron substrate.

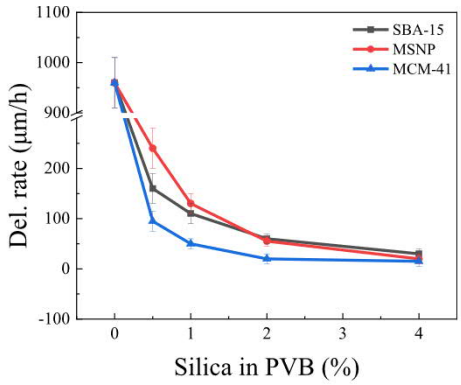

Fig. 11. Averaged delamination rates for PVB coatings containing different mesoporous silica coated on Fe substrate during the monitoring regions. Although the delamination progress observed for PVB/Fe shows a sqrt(t) time dependence, for easier comparison with the rates shown in the figure also a linear rate was determined from averaging over the first 3 h, and that gives about 960 μm/h, i.e. much higher than the rates observed even for the lowest addition of silica.

delamination distance is just around 1 mm in 60 h. For PVB containing 2% or 4% MCM-41, the delamination rates are nearly the same, i.e. 20 μm/h and 15 μm/h, respectively. That means further increase the amount of MCM-41 is not expected to further decrease the delamination rate, i.e. for MCM-41 2% can be considered as a critical concentration. For SBA-15 and MSNP this critical concentration seems to be higher than for MCM-41, i.e. rather 4%. So, the delamination rate is determined by the type of the mesoporous silica and the concentration of mesoporous silica in the coating (see Fig. 11).

Quantifying the effect on cathodic delamination rate, by increasing the mesoporous silica content from 0.5% to 4% additions into the PVB coating reduced the delamination rate from 240 μm/h to 15 μm/h. The cathodic delamination rates were reduced by 4–64 times compared to unpigmented PVB with a delamination rate of 960 μm/h (see Fig. 5(b)). That means the mesoporous silica in the PVB coating can significantly inhibit the cathodic delamination rate to protect the Fe substrate. Of the three type of mesoporous silica, the MCM-41 filler shows the best corrosion inhibition property and that already at lower added amount than the other two mesoporous silica.

Different from PVB with silica additions applied on Zn, on Fe substrate just the delamination rate is decreased, but no indications for a restoration of a blocking interface are observed in the cathodic delamination profiles, even not for the low concentration of 0.5%. Inhibition by silica particle addition to organic coatings applied on Fe was also observed in other studies, even though not to the same high extent [14, 18].

Since cathodic delamination is mainly determined by the interfacial structure and composition, especially at the delamination front, the question is what the effect of silica particles at this interface could be. It is reasonable to assume that the particles in the PVB coating might quite likely have an effect on decreasing diffusion of water and ions vertically from the coating surface to the buried interface. An effect of silica additions on lateral diffusion is not that obvious, although there are reports about an improved interfacial adhesion [14]. There are quite a number of publications where higher cross-linking as well as filling of pores and cracks by inert fillers such as silica is postulated [11–18]. Size and shape as well as surface properties might play a role in this. In addition, it can be assumed that during cathodic delamination at the delamination front as well as at the delaminating interface silica particles in the vicinity of the metal surface are exposed to the increase of pH which is a consequence of oxygen reduction at the delaminating and delaminated interface. This increase in pH will be more pronounced on iron than on zinc, because on iron the increase in pH is much larger. The increase in pH will result in degradation of the silica. The degradation of silica is directly dependent on the pH, the degradation product in the solution can be H_4SiO_4, $H_3SiO_4^-$, and $H_2SiO_4^{2-}$ [56–59]. At pH values below 7, the solubility of silica is low, but around pH 11 the dominant species is $H_3SiO_4^-$, and it is $H_2SiO_4^{2-}$ when the pH above 11.

It is hence assumed that at high pH levels no stable silicate layer can

be formed, i.e. that for iron the corresponding degradation products can only adsorb on the iron surface and lead there to an inhibition of further delamination at the delamination front. As not much of these degradation products might be needed there, the effect is nearly immediate, but does not lead to a self-healing of the already delaminated interface. For the latter it is necessary that the gap formed by delamination between coating and metal surface is closed again by a new solid phase. It is proposed here that this is occurring for the case of zinc as substrate. Contrary to iron which stays passive during cathodic delamination, zinc does corrode under these conditions. This leads to a lower increase of pH, which makes it more likely that the buffering effect of silica degradation (see Eq. (1) and Eq. (2)) on top of the one of Zn^{2+}, which buffers pH by forming hydroxides, might be enough to allow formation of stable silicate layers, maybe alongside stable zinc corrosion products. It is possible that Zn cations are also part of the silicate layer (see Eq. (3)).

$$2OH^- + SiO_2 \rightarrow H_2SiO_4^{2-} \text{ or } H_2O + OH^- + SiO_2 \rightarrow H_3SiO_4^- \quad (1)$$

Maybe more instructive is the view on the siloxane bonds in the silica particle:

$$\equiv Si–O–Si\equiv + OH– \rightarrow \equiv Si–OH + –O–Si\equiv \quad (2)$$

These degradation products can react with Zn cations or hydroxides, such as e.g.:

$$Zn(OH)^+ + H_3SiO_4^- \rightarrow ZnSiO_3{\cdot}2\,H_2O \downarrow \quad (3)$$

Hence precipitation of a corrosion product layer formed by potassium cations from the defect and on zinc also by zinc cations and/or zinc hydroxides (see Eq. (3)) and the silicates released by the degrading silica might take place, if the pH is sufficiently buffered. This is proposed here to indeed occur on zinc and, if sufficiently high amounts of silicate zinc or zinc hydroxide ions are available, to lead to the pronounced self-healing observed for PVB on zinc with additions of 0.5% SBA-15 or MCM-41. On iron the pH levels might not be enough buffered to form a fully protective layer that also blocks ion transport between defect and interface. Fig. 12 show schematically the difference in silicate layer formation at the delaminated interface on zinc and on iron for mesoporous silica containing PVB coatings.

Concerning the effect of size and concentration of the silica particles, for these lower silica contents the fast initial delamination and the correlated initial high activity of ORR (oxygen reduction reaction) and zinc (oxide) dissolution at the delaminated interface provides sufficient amounts of corrosion products for this self-healing at the interface, which obviously sets in very immediate, most likely triggered once buffering is significant enough and the pH is lowered beneath a certain threshold. At higher amounts, it is proposed that improved cross-linking in the PVB and maybe also higher adhesion caused by the silica are one factor for the more or less immediate inhibition of delamination, as proposed also e.g. by Fernández-Álvarez et al. [18]. Most likely also an immediate initial release of a lower amount of degradation products of silica may occur, contributing to a significant inhibition of delamination, which prevents, however, formation of enough corrosion product to result in self-healing of the already (partially) delaminated interface. This is also the case for 0.5% of MSNP in the PVB applied on zinc. There the delamination is obviously inhibited too significantly right from the beginning. On iron the high pH levels reached there due to absence of buffering by dissolved iron cations, because iron is stable at the high pH levels caused by ORR, prevent the formation of a stable silicate layer that can restore the interface again. It is striking that MSNP has the strongest inhibitive effect right from the beginning on zinc, while it has the smallest initial effect on iron. It is assumed that the explanation for this lies in the difference in pH on Zn compared to Fe and how this leads to degradation of the silica. It is reasonable to assume that the pH increase is initially mainly localized in a relatively thin layer directly at the interface and that this will be thinner for zinc than for iron as substrate. For larger particles, initially less silica degradation might occur, as only part of a particle is in that layer of sufficiently increased pH, but then more, once the whole particle degrades. For smaller particles, all particles in that layer will get quickly activated, leading to an initial higher release rate, but no further degradation will occur. This might be what leads to the observed behavior on zinc. On iron the threshold for inhibition might be different and the higher initial release of the smaller particles has hence also a higher initial effect. In order to investigate the resulting silicate layers in more detail, surface analytical investigations of the interface were carried out.

3.3. XPS depth profiles

XPS was used to investigate the interfacial layer of silicate-based corrosion products forming at the polymer/zinc interface as consequence of cathodic delamination. Fig. 13 (a, b, c) shows XPS Si detail spectra for different sputtering depths of the intact interface and the delaminated interface after removal of PVB coatings containing 0.5% additions of the three different silica types, after cathodic delamination experiments were carried out. Since adhesion of PVB to zinc is not very high, it is not too difficult to remove it from the substrate, especially in the delaminated, albeit restored area. The high-resolution spectra obtained on the zinc substrate in the delaminated area reveal the presence of Si at the delaminated interface. The existence of Si shows that the

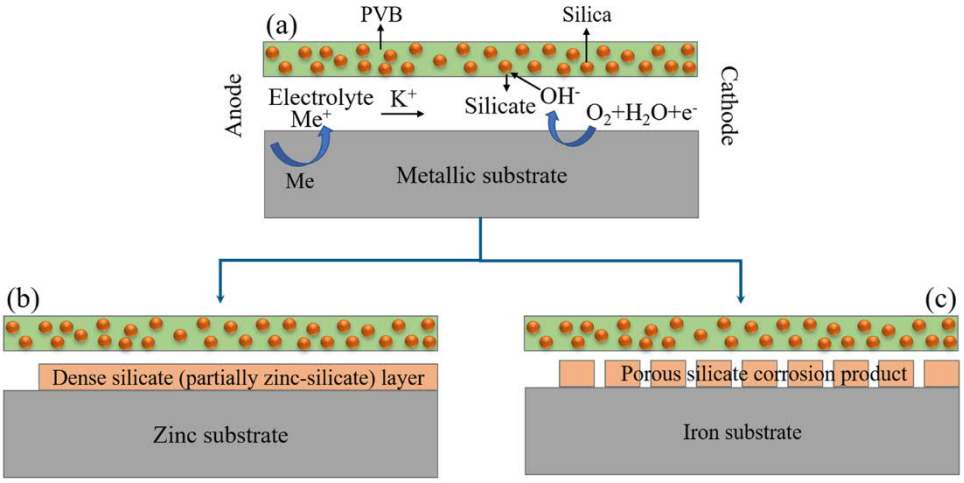

Fig. 12. Schematic representation of the corrosion-driven cathodic delamination. (a) Typical degradation product formation, (b) on zinc substrate and (c) on iron substrate.

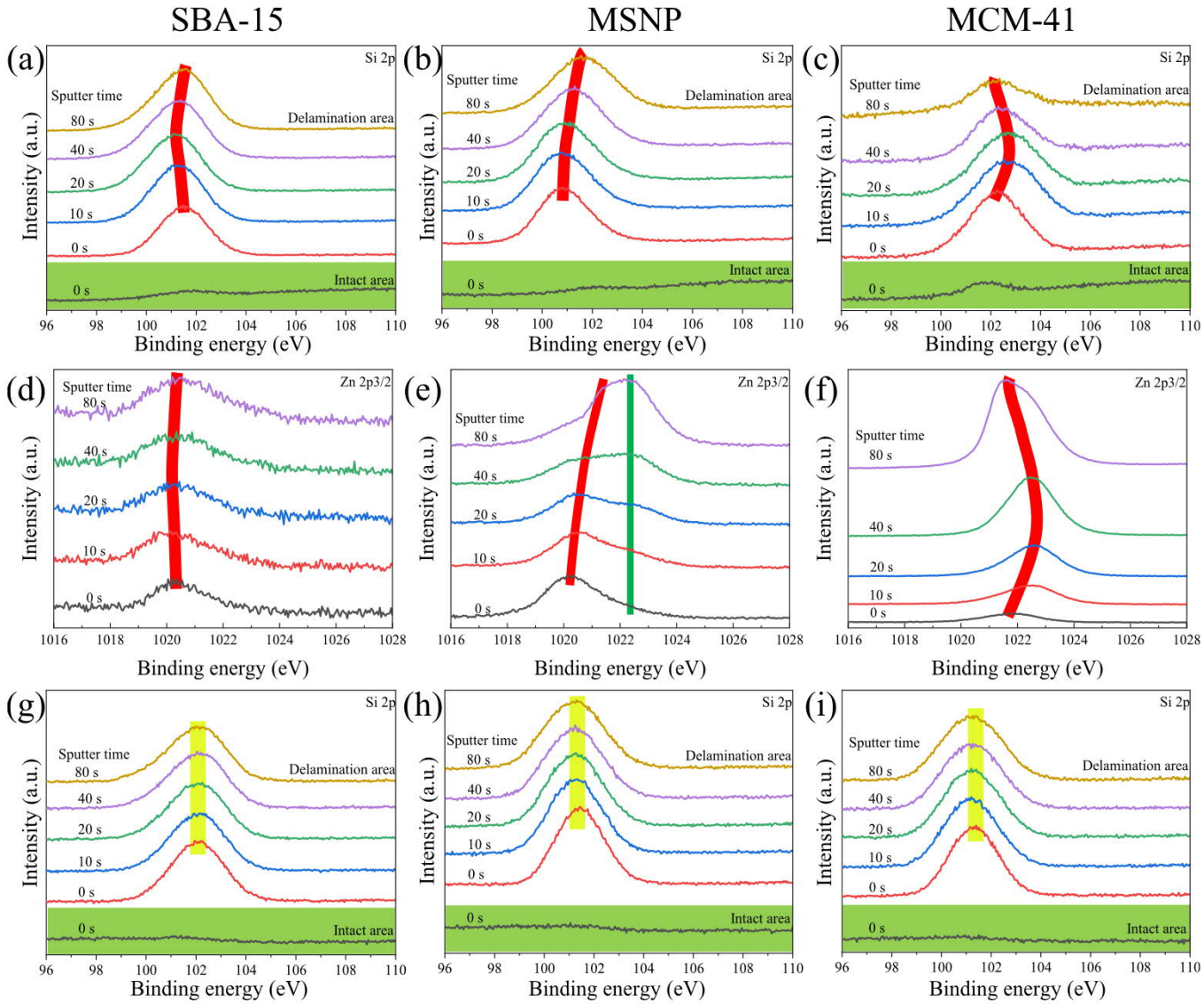

Fig. 13. Si and zinc signal obtained via XPS depth profiles carried out at the delaminated surface after removal of the coating. 0.5% mesoporous silica in PVB coated on Zn or Fe substrate. (a, b, c) Zn substrate, (g, h, i) Fe substrate. (d, e, f) show the Zn 2p3/2 peaks corresponding to (a, b, c). Note the shifts in peak position that are observed on zinc (highlighted by red line, note the non-shifting peak in (e) marked in dark green), indicating the more insulating nature of the resulting silicate layer. (For interpretation of the references to colour in this figure, the reader is referred to the web version of this article.)

mesoporous SiO_2 close to the interface at least partially degrades during the delamination process. In the intact area no Si can be detected, as to be expected for the intact interface.

Fig. 13 (g, h, i) shows the XPS survey spectra obtained from the initial surface and after depth profiling obtained on samples of (partially delaminated) PVB coatings containing mesoporous SiO_2 additives applied on iron substrate. Also, here significant amounts of Si can be found even after 80 s of sputtering (about 10 nm) in the delaminated area.

For both substrates the results indicate that a thick layer of silica degradation products is forming during delamination of the coatings on both substrates. The crucial point here is that on zinc as substrate zinc cations are incorporated into this layer, indicating the presence of zinc silicate (see Fig. 13 (d, e, f)). For 0.5% SBA-15 added to the PVB, only small amounts of Zn are found, however. This is attributed to the fact that for SBA-15 the restoration of the interface is by far the fastest, giving only little time (about 4 h) for zinc corrosion at the interface before the protective corrosion product layer is formed. For 0.5% MCM-41 addition to the PVB on Zn, it takes much longer (about 16 h), which should result in a significantly higher amount of zinc dissolved. For MSNP no fully protecting interface, that is able to inhibit ion migration between defect and delaminated interface, is formed at all. This explains the differences in the amounts of Zn found in the sputter profiles. Since for SBA-15 this layer is obviously the most protective, the presence of zinc is not the main reason for the protective nature of the formed layer. It is rather assumed that the degree of pH buffering as a consequence of silica degradation in combination with the already lower pH than on iron is rather what is important.

On iron, only a non-protective degradation product layer is forming. Since the iron does not corrode under the conditions of cathodic delamination, iron cations are not part of this layer. The difference in the protective qualities of the interfacial corrosion product layers forming on iron and zinc are suggested here to be reflected in the peaks shifts of the Si 2p XPS signal, as they are observed on zinc, but not on Fe. This indicates a more insulating nature of the corrosion product layer on Zn.

That the observed shift of the Si peak is most likely a consequence of charging is supported by an analysis of the corresponding Zn 2p3/2 peaks:

First of all, the peak obtained on the layer formed in the presence of MSNP in the PVB seems to consist of two peaks, one at 1020 eV and one

at 1022 eV (see Fig. 13 (e)). However, it seems unlikely that these indicate indeed two different kind of Zn in the layer, as the binding energies for the peak in zinc oxides and silicates are quite similar, around 1022 eV. It is hence assumed that these seemingly two peaks are rather indicating that there are protective, insulating regions in the layer, and non-protective, non-insulating ones. The peak assumed to correspond to the insulating regions shows a similar shift as the Si peak (highlighted by red in Fig. 13 (e) and to be compared with the shift in the Si 2p peak in Fig. 13 (b)). That only part of the peak shifts, the other stays at about 1022 eV, means that only a part of the layer is insulating. This is in good agreement with the observation that this layer does not lead to a restoration of a protective interface. For MCM-41 (see Fig. 13 (f)), a similar peak shift is observed as for the corresponding Si peak, confirming the insulating nature of this layer. As mentioned, for SBA-15 (Fig. 13 (d)) only little Zn intensity was found.

3.4. The degradation of mesoporous silica

In order to mimic the underfilm alkaline condition, an immersion experiment to degrade mesoporous SiO_2 under alkaline condition was performed. During the delamination process, the cathodic oxygen reduction reaction at the delaminating and delaminated interface will produce OH^-, which leads to an increase of the pH value in these areas, with values as high as pH 10–11 for zinc have been recorded [60–62], and even higher for iron [30]. This difference could also play a role on the protective quality of the two different degradation product layers. In order to simulate the condition at the underfilm corrosion, a 1 M KCl solution with pH 10 was used to dissolve mesoporous SiO_2. Fig. 14 shows the dissolution curve of mesoporous SiO_2 for immersion times of up to 6 days at room temperature where the Si content in the solution was evaluated by ICP-OES. The dissolution of the three different types of mesoporous SiO_2 shows a similar behavior for all: an initial period of slow dissolution which increases gradually with time. Finally, a maximum solubility is reached. A similar initial period of slow SiO_2 dissolution was also observed in other works [63,64]. The corresponding concentration of the maximum soluble Si is about 35 mg/l. However, the total amount of Si dissolution of SBA-15 is slightly lower than compared to MCM-41 or MSNP during this latter stage. It is known that the degradation of the SiO_2 occurs via rupture of the Si—O bond which is strongly dependent on pH. In alkaline condition, OH^- ions will catalytically promote deprotonation of silanol groups and hydrolysis of Si—O—Si bonds to increase the dissolution of SiO_2 [63]. Fig. 14 clearly demonstrates that even under quite mild alkaline conditions the dissolution of silica occurs at quite significant rates. At higher pH values it will be even faster. No direct correlation between particle size and the dissolved amount was observed here. However, the results obtained in the delamination experiments show that there is a dependence on size and maybe also shape. This is assumed to be rather due to the corresponding effect on release rates of degradation products. Silica of different size and shapes distributed in the polymer matrix will result in different initial and overall release rates. As already mentioned above, it is proposed here that for Zn as substrate, where the zone of increased pH vertically from the surface into the coating will be relatively narrow, for the smallest size initially the highest release is expected. But on the long run larger particles of which just parts are in that zone will most likely at least partly degrade also in the parts outside that zone and thus supply more degradation products. On iron where the zone of high pH is thicker, this is different.

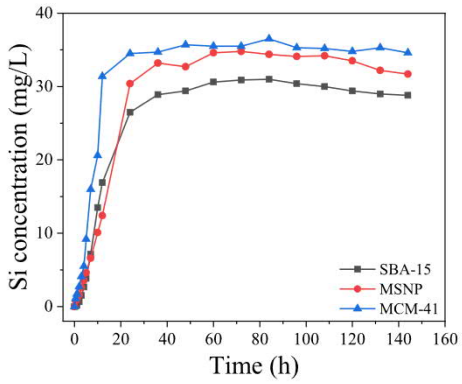

Fig. 14. Dissolution curves measured for different mesoporous silica in 1 M KCl (pH 10).

4. Conclusions

In this work the effect of different kinds of mesoporous silica used as additions to PVB organic coatings applied on both zinc and iron on improving the resistance against cathodic delamination was investigated. It was found that:

(1) The addition of mesoporous silica in the PVB coating applied onto zinc can significantly decrease the cathodic delamination rate. More precisely it significantly decreases the delamination for additions of 1% or more. For lower concentrations of 0.5%, the effect for the case of MSNP was relatively small, but for MCM-41 or SBA-15 a very interesting behaviour was observed. While initially the delamination occurs nearly as usual, after a few hours (and several millimeters of delamination) self-healing at the interface was observed, i.e. delamination not only came to a halt but the potential at the delaminated interface increased again to the one of passive zinc. Since the defect remains active, i.e. no corrosion inhibition occurs in the defect, this means that the delaminated interface was re-established into an interface effectively blocking ion transfer and inhibiting electrochemical reactions. Such behavior is of high interest for smart self-healing coatings where a relatively fast delamination progress ensures fast spreading of a trigger signal (e.g. increase in pH, decrease in potential) for smart release as well as fast transport of the released active agents along the delaminated interface. Once the defect is passivated and maybe even covered by a new polymer coating, the delaminated interface has to be healed, too. This is obviously provided by the silica additions to the coating. It is proposed that as a consequence of the cathodic ORR at the delaminated and delaminating interface the corresponding increase of pH leads to a degradation of the silica in the vicinity of the interface. The silicate released by this degradation forms a protective layer and re-established a protective interface.

(2) For such silica containing PVB coatings applied on Fe substrate, just a decrease of the cathodic delamination rate is observed, but no self-healing of the interface. Even though also in this case a thick layer of degradation products of the resulting layer is found to be less protective. This is proposed to be mainly related to the initially much higher pH values at the interface, which is proposed to result in a more porous corrosion product layer that cannot block ion transport between defect and the delaminated interface.

(3) The size of mesoporous SiO_2 seems to have an effect on the degree of inhibition of the cathodic delamination rate. For iron as substrate it is observed that with increasing size of the mesoporous SiO_2 particles in the PVB coating, the decrease of the rate of cathodic delamination is more pronounced. The coating with 4% MCM-41 shows the best corrosion resistance and lowest cathodic delamination. To the contrary, for zinc as substrate, the initial inhibition effect is the strongest for the smallest silica particles. It is proposed that this is due to the effect that on zinc the interfacial zone of significantly increased pH is much thinner than on iron. In this case a higher release rate of silicate is proposed to occur only for the smaller particles. The larger particles are not fully

inside this thin layer of higher pH and hence show initially a lower degradation rate. However, this higher initial inhibition for the smallest particles is proposed to be the reason that at 0.5% silica addition the smallest silica particles (MSNP) do not show a self-healing of the delaminated interface, while the others do. It is proposed that the higher initial inhibition of cathodic delamination for PVB with 0.5% MSNP prevents sufficient silica degradation and maybe also zinc corrosion as to allow the formation of a blocking corrosion product layer at the interface that restores it as intact interface. This is also proposed to be the reason for the absence of self-healing at higher additions of silica in general. The degradation in alkaline aqueous solution did not reveal any significant differences between the different particles.

Concluding, the corrosion behavior of organic coatings can be effectively improved through addition of mesoporous SiO_2. The amount and size of the added mesoporous SiO_2 plays an important role for the overall performance. It is believed that the present work will give important guidance on how to apply mesoporous SiO_2 for significantly improving self-healing coatings in the future. Especially for application on zinc the observed self-healing effect at the delaminated interface is very promising for application in smart self-healing coatings.

CRediT authorship contribution statement

Yue Yin: Conceptualization, Validation, Investigation, Methodology, Writing – original draft, Writing – review & editing. **Huan Zhao:** Methodology, Validation. **Manoj Prabhakar:** Methodology, Validation. **Michael Rohwerder:** Supervision, Conceptualization, Validation, Writing – review & editing.

Declaration of Competing Interest

The authors declare that they have no known competing financial interests or personal relationships that could have appeared to influence the work reported in this paper.

Acknowledgments

Yue Yin would like to acknowledge the financial support from the China Scholarship Council.

Council and also the Max-Planck Society for partial funding. We thank Petra Ebbinghaus for the FTIR, Daniel Kurz for the ICP-OES measurements.

References

[1] I. Milosev, G.S. Frankel, Review-conversion coatings based on zirconium and/or titanium, J. Electrochem. Soc. 165 (2018) C127–C144.
[2] M. Rohwerder, Conducting polymers for corrosion protection: A review, Int. J. Mater. Res 100 (2009) 1331–1342.
[3] M.L. Zheludkevich, I.M. Salvadob, M.G.S. Ferreira, Sol-gel coatings for corrosion protection of metals, J. Mater. Chem. 15 (2005) 5099–5111.
[4] F. Zhang, P.F. Ju, M.Q. Pan, D.W. Zhang, Y. Huang, G.L. Li, X.G. Li, Self-healing mechanisms in smart protective coatings: A review, Corros. Sci. 144 (2018) 74–88.
[5] F. Presuel-Moreno, M.A. Jakab, N. Tailleart, M. Goldman, J.R. Scully, Corrosion-resistant metallic coatings, Mater. Today 11 (2008) 14–23.
[6] R.B. Figueira, C.J.R. Silva, E.V. Pereira, Organic-inorganic hybrid sol-gel coatings for metal corrosion protection: a review of recent progress, J. Coat. Technol. Res. 12 (2015) 1–35.
[7] K. Pélissier, D. Thierry, Powder and high-solid coatings as anticorrosive solutions for marine and offshore applications? A review, Coatings 10 (2020) 916.
[8] R.G. Hu, S. Zhang, J.F. Bu, C.J. Lin, G.L. Song, Recent progress in corrosion protection of magnesium alloys by organic coatings, Prog. Org. Coat. 73 (2012) 129–141.
[9] P.A. Sørensen, S. Kiil, K. Dam-Johansen, C.E. Weinell, Anticorrosive coatings: a review, J. Coat. Technol. Res. 6 (2009) 135–176.
[10] A.V. Radhamani, H.C. Lau, S. Ramakrishna, Nanocomposite coatings on steel for enhancing the corrosion resistance: A review, J. Compos. Mater. 54 (2020) 681–701.
[11] Y.S.H. Xu, D.M. Gao, Q. Dong, M.H. Li, A.Q. Liu, X.C. Wang, S.F. Wang, Q. Liu, Anticorrosive behavior of epoxy coating modified with hydrophobic nano-silica on phosphatized carbon steel, Prog. Org. Coat. 151 (2021), 106051.
[12] J.P. Lu, L. Chen, R.G. Song, Effects of SiO_2 particle size on the corrosion resistance of fluoropolymer/SiO_2 composite coatings, Surf. Eng. 35 (2019) 440–449.
[13] M.A. El-Fattah, A.M. El-Saeed, R.A. El-Ghazawy, Chemical interaction of different sized fumed silica with epoxy via ultrasonication for improved coating, Prog. Org. Coat. 129 (2019) 1–9.
[14] C.L. Zhou, X. Lu, Z. Xin, J. Liu, Y.F. Zhang, Polybenzoxazine/SiO_2 nanocomposite coatings for corrosion protection of mild steel, Corros. Sci. 80 (2014) 269–275.
[15] N. Wang, K.Q. Cheng, H. Wu, C. Wang, Q.C. Wang, F.H. Wang, Effect of nano-sized mesoporous silica MCM-41 and MMT on corrosion properties of epoxy coating, Prog. Org. Coat. 75 (2012) 386–391.
[16] M.F. Montemor, A.M. Cabral, M.L. Zheludkevich, M.G.S. Ferreira, The corrosion resistance of hot dip galvanized steel pretreated with bis-functional silanes modified with microsilica, Surf. Coat. Technol. 200 (2006) 2875–2885.
[17] V. Palanivel, D.Q. Zhu, W.J. Van, Ooij, Nanoparticle-filled silane films as chromate replacements for aluminum alloys, Prog. Org. Coat. 47 (2003) 384–392.
[18] M. Fernández-Álvarez, F. Velasco, A. Bautista, Y. Gonzalez-Garcia, B. Galiana, Corrosion protection in chloride environments of nanosilica containing epoxy powder coatings with defects, J. Electrochem. Soc. 167 (2020), 161507.
[19] Y. Zhao, L.P. Lv, S. Jiang, K. Landfester, D. Crespy, Advanced stimuli-responsive polymer nanocapsules with enhanced capabilities for payloads delivery, Polym. Chem. 6 (2015) 4197–4205.
[20] M.F. Montemor, Functional and smart coatings for corrosion protection: A review of recent advances, Surf. Coat. Technol. 258 (2014) 17–37.
[21] J.M. Falcón, L.M. Otubo, I.V. Aoki, Highly ordered mesoporous silica loaded with dodecylamine for smart anticorrosion coatings, Surf. Coat. Technol. 303 (2016) 319–329.
[22] M. Stempniewicz, M. Rohwerder, F. Marlow, Release from silica SBA-3-like mesoporous fibers: Cross-wall transport and external diffusion barrier, ChemPhysChem 8 (2007) 188–194.
[23] Y. Yin, M. Schulz, M. Rohwerder, Optimizing smart self-healing coatings: Investigating the transport of active agents from the coating towards the defect, Corros. Sci. 190 (2021), 109661.
[24] L.W. Ma, J.K. Wang, D.W. Zhang, Y. Huang, L.Y. Huang, P.J. Wang, H.C. Qian, X. G. Li, H.A. Terryn, J.M.C. Mol, Dual-action self-healing protective coatings with photothermal responsive corrosion inhibitor nanocontainers, Chem. Eng. Sci. 404 (2021), 127118.
[25] E.V. Skorb, D. Fix, D.V. Andreeva, H. Möhwald, D.G. Shchukin, Surface-modified mesoporous SiO_2 containers for corrosion protection, Adv. Funct. Mater. 19 (2009) 2373–2379.
[26] P. Loison, V. Debout, H. Groult, J. Creus, S. Touzain, Incorporation of silica nanocontainers and its impact on a waterborne polyurethane coating, Mater. Corros. 70 (2019) 1884–1899.
[27] A. Vimalanandan, L.P. Lv, T.H. Tran, K. Landfester, D. Crespy, M. Rohwerder, Redox responsive self-healing for corrosion protection, Adv. Mater. 25 (2013) 6980–6984.
[28] T.H. Tran, A. Vimalanandan, G. Genchev, J. Fickert, K. Landfester, D. Crespy, M. Rohwerder, Regenerative nano-hybrid coating tailored for autonomous corrosion protection, Adv. Mater. 27 (2015) 3825–3830.
[29] D.R. Radu, C.Y. Lai, K. Jeftinija, E.W. Rowe, S. Jeftinija, V.S.Y. Lin, A polyamidoamine dendrimer-capped mesoporous silica nanosphere-based gene transfection reagent, J. Am. Chem. Soc. 126 (2004) 13216–13217.
[30] A. Leng, H. Streckel, M. Stratmann, The delamination of polymeric coatings from steel. Part 1: Calibration of the Kelvin probe and basic delamination mechanism, Corros. Sci. 41 (1999) 547–578.
[31] D.Y. Zhao, J.L. Feng, Q.S. Huo, N. Melosh, G.H. Fredrickson, B.F. Chmelka, G. D. Stucky, Triblock copolymer syntheses of mesoporous silica with periodic 50 to 300 angstrom pores, Science 279 (1998) 548–552.
[32] H. Sanaeishoar, M. Sabbaghan, F. Mohave, Synthesis and characterization of micro-mesoporous MCM-41 using various ionic liquids as co-templates, Microporous Mesoporous Mater. 217 (2015) 219–224.
[33] L. Baptista de Oliveira Freitas, I.J. Gonzalez Bravo, W.A. de Almeida Macedo, E. Martins, Barros de Sousa, Mesoporous silica materials functionalized with folic acid: preparation, characterization and release profile study with methotrexate, J. Sol-Gel Sci. Technol. 77 (2016) 186–204.
[34] H.I. Hsiang, C.C. Chen, J.Y. Tsai, Dispersion of nonaqueous Co_2Z ferrite powders with titanate coupling agent and poly(vinyl butyral), Appl. Surf. Sci. 245 (2005) 252–259.
[35] P. Peer, M. Stenicka, V. Pavlinek, P. Filip, I. Kuritka, J. Brus, An electrorheological investigation of PVB solutions in connection with their electrospinning qualities, Polym. Test. 39 (2014) 115–121.
[36] A.U. Chaudhry, V. Mittal, B. Mishra, Inhibition and promotion of electrochemical reactions by graphene in organic coatings, RSC Adv. 5 (2015) 80365–80368.
[37] M.V. Pergal, J. Brkljacic, G. Tovilovic-Kovacevic, M. Spirkova, I.D. Kodranov, D. D. Manojlovic, S. Ostojic, N.Z. Knezevic, Effect of mesoporous silica nanoparticles on the properties of polyurethane network composites, Prog. Org. Coat. 151 (2021), 106049.
[38] N. Wang, N. Gao, S. Jiang, Q.H. Fang, E.F. Chen, Effect of different structure MCM-41 fillers with PP-g-MA on mechanical and crystallization performances of polypropylene, Compos. B. Eng. 42 (2011) 1571–1577.
[39] G. Williams, H.N. McMurray, Inhibition of corrosion driven delamination on iron by smart-release bentonite cation-exchange pigments studied using a scanning Kelvin probe technique, Prog. Org. Coat. 102 (2017) 18–28.

[40] R.J. Holness, G. Williams, D.A. Worsley, H.N. McMurray, Polyaniline inhibition of corrosion-driven organic coating cathodic delamination on iron, J. Electrochem. Soc. 152 (2005) B73–B81.
[41] G. Williams, S. Geary, H.N. McMurray, Smart release corrosion inhibitor pigments based on organic ion-exchange resins, Corros. Sci. 57 (2012) 139–147.
[42] G. Williams, H.N. McMurray, D.A. Worsley, Cerium (III) inhibition of corrosion-driven organic coating delamination studied using a scanning kelvin probe technique, J. Electrochem. Soc. 149 (2002) B154–B162.
[43] G. Williams, A. Gabriel, A. Cook, H.N. McMurray, Dopant effects in polyaniline inhibition of corrosion-driven organic coating cathodic delamination on iron, J. Electrochem. Soc. 153 (2006) B425–B433.
[44] C.F. Glover, G. Williams, Inhibition of corrosion-driven organic coating delamination and filiform corrosion on iron by phenyl phosphonic acid, Prog. Org. Coat. 102 (2017) 44–52.
[45] R. Hausbrand, M. Stratmann, M. Rohwerder, The physical meaning of electrode potentials at metal surfaces and polymer/metal interfaces: Consequences for delamination, J. Electrochem. Soc. 155 (2008) C369–C379.
[46] B.E. Conway, D.C.W. Kannangara, Zinc oxidation and redeposition processes in aqueous alkali and carbonate solutions: II. Distinction between dissolution and oxide film formation processes, J. Electrochem. Soc. 134 (1987) 906–918.
[47] M. Mokaddem, P. Volovitch, K. Ogle, The anodic dissolution of zinc and zinc alloys in alkaline solution. I. Oxide formation on electrogalvanized steel, Electrochim. Acta 55 (2010) 7867–7875.
[48] A. Merz, M. Uebel, M. Rohwerder, The protection zone: A long-range corrosion protection mechanism around conducting polymer particles in composite coatings: part I. polyaniline and polypyrrole, J. Electrochem. Soc. 166 (2019) C304–C313.
[49] J.S. Mondragon-Ochoa, A. Altin, J. Rechmann, A. Erbe, Delamination kinetics of thin film poly(acrylate) model coatings prepared by surface initiated atom transfer radical polymerization on iron, J. Electrochem. Soc. 165 (2018) C991–C998.
[50] M. Stratmann, M. Wolpers, H. Streckel, R. Feser, Use of a scanning-kelvinprobe in the investigation of electrochemical reactions at the metal/polymer interface, Ber. Der Bunsenges. Für Phys. Chem. 95 (1991) 1365–1375.
[51] M. Stratmann, A. Leng, W. Fürbeth, H. Streckel, H. Gehmecker, K.H. Große-Brinkhaus, The scanning Kelvin probe; a new technique for the in situ analysis of the delamination of organic coatings, Prog. Org. Coat. 27 (1996) 261–267.
[52] A. Leng, H. Streckel, M. Stratmann, The delamination of polymeric coatings from steel. Part 2: first stage of delamination, effect of type and concentration of cations on delamination, chemical analysis of the interface, Corros. Sci. 41 (1998) 579–597.
[53] W. Fürbeth, M. Stratmann, The delamination of polymeric coatings from electrogalvanized steel–a mechanistic approach. Part 3: delamination kinetics and influence of CO_2, Corros. Sci. 43 (2001) 243–254.
[54] N. Wint, C.M. Griffiths, C.J. Richards, G. Williams, H.N. McMurray, The role of benzotriazole modified zinc phosphate in preventing corrosion driven organic coating disbondment on galvanised steel, Corros. Sci. 174 (2020), 108839.
[55] J.M. Prabhakar, P. Kerger, A. de Vooys, M. Rohwerder, Migration of ions on oxygen-deficient chromium oxide electrodeposited from trivalent chromium electrolyte, Corros. Sci. 199 (2022), 110185.
[56] H. Li, Z.A. Zhou, Z. Xu, J.H. Masliyah, Role of acidified sodium silicate in low temperature bitumen extraction from poor-processing oil sand ores, Ind. Eng. Chem. Res. 44 (2005) 4753–4761.
[57] X.F. Yang, P. Roonasi, A. Holmgren, A study of sodium silicate in aqueous solution and sorbed by synthetic magnetite using in situ ATR-FTIR spectroscopy, J. Colloid Interface Sci. 328 (2008) 41–47.
[58] C. Brinker, G. Scherer, Sol-gel science. The Physics and Chemistry of Sol-gel Processing, Academic Press, New York, 1990.
[59] M.E. Simonsen, C. Sønderby, Z.S. Li, E.G. Søgaard, XPS and FT-IR investigation of silicate polymers, J. Mater. Sci. 44 (2009) 2079–2088.
[60] W. Fürbeth, M. Stratmann, Scanning Kelvin probe investigations on the delamination of polymeric coatings from metallic surfaces, Prog. Org. Coat. 39 (2000) 23–29.
[61] G. Williams, H.N. McMurray, Chromate inhibition of corrosion-driven organic coating delamination studied using a scanning kelvin probe technique, J. Electrochem. Soc. 148 (2001) B377–B385.
[62] W. Fürbeth, M. Stratmann, The delamination of polymeric coatings from electrogalvanized steel-a mechanistic approach.: part 1: delamination from a defect with intact zinc layer, Corros. Sci. 43 (2001) 207–227.
[63] K. Braun, A. Pochert, M. Beck, R. Fiedler, J. Gruber, M. Linden, Dissolution kinetics of mesoporous silica nanoparticles in different simulated body fluids, J. Sol-Gel Sci. Technol. 79 (2016) 319–327.
[64] Q.J. He, J.L. Shi, M. Zhu, Y. Chen, F. Chen, The three-stage in vitro degradation behavior of mesoporous silica in simulated body fluid, Microporous Mesoporous Mater. 131 (2010) 314–320.